JOURNAL OF GEOPHYSICAL RESEARCH, VOL. 98, NO. A11, PAGES 19,381–19,393, NOVEMBER 1, 1993

Decay of Equatorial Ring Current Ions and Associated Aeronomical Consequences

M.-C. FOK, J. U. KOZYRA, A. F. NAGY, C. E. RASMUSSEN, AND G. V. KHAZANOV

Space Physics Research Laboratory, Department of Atmospheric, Oceanic and Space Sciences, University of Michigan, Ann Arbor

The decay of the major ion species which constitute the ring current is studied by solving the time evolution of their distribution functions during the recovery phase of a moderate geomagnetic storm. In this work, only equatorially mirroring particles are considered. Particles are assumed to move subject to E×B and gradient drifts. They also experience losses along their drift paths. Two loss mechanisms are considered: charge exchange with neutral hydrogen atoms and Coulomb collisions with thermal plasma in the plasmasphere. Thermal plasma densities are calculated with a plasmaspheric model employing a time-dependent convection electric field model. The drift-loss model successfully reproduces a number of important and observable features in the distribution function. Charge exchange is found to be the major loss mechanism for the ring current ions; however the important effects of Coulomb collisions on both the ring current and thermal populations are also presented. The model predicts the formation of a low-energy (< 500 eV) ion population as a result of energy degradation caused by Coulomb collisions of the ring current ions with the plasmaspheric electrons; this population may be one source of the low-energy ions observed during active and quiet periods in the inner magnetosphere. The energy transferred to plasmaspheric electrons through Coulomb collisions with ring current ions is believed to be the energy source for the electron temperature enhancement and the associated 6300 Å (stable auroral red [SAR] arc) emission in the subauroral region. The calculated energy-deposition rate is sufficient to produce a subauroral electron temperature enhancement and SAR arc emissions that are consistent with observations of these quantities during moderate magnetic activity levels.

1. Introduction

In this work we study processes that occur during the recovery phase of a moderate geomagnetic storm. The ring current has already formed as a consequence of processes which have occurred during the main phase [*Chen et al.*, 1993]. The recovery phase is associated with the decay of the ring current. Three loss mechanisms have been suggested: (1) charge exchange with the neutral hydrogen; (2) Coulomb collisions with thermal plasma in the plasmasphere; (3) pitch angle diffusion into the atmospheric loss cone as a result of wave-particle interactions. The time evolution of the energy spectra of ring current ions after storm injection was studied by *Kistler et al.* [1989]. They only considered the charge exchange loss of ring current ions along the drift path. Their predicted spectra agreed reasonably well with measurements at high energies, but there were disagreements at energies below 5 keV. In this paper the decay of the major ion species (H^+, He^+, and O^+) making up the ring current is studied, considering drift motion, charge exchange loss, and also Coulomb drag during the recovery phase of a moderate magnetic storm with maximum *Kp* of 6.

The effect of Coulomb collisions on ring current ions is studied by solving the Fokker-Planck equation. Energetic ring current ions are slowed down by thermal plasma in the plasmasphere via Coulomb collisions. Usually, Coulomb collisions are considered as a minor loss of ring current ions when compared with charge exchange losses. However, the Coulomb decay lifetime is comparable with or less than the charge exchange lifetime for energies below ~10 keV [*Fok et al.*, 1991*b*]. The inclusion of Coulomb collisions does change the distribution function significantly at low energies. A low-energy (< 500 eV) ion population is formed as a result of the energy degradation, via Coulomb collisions, of the high-energy ring current ions. Furthermore, the ring current energy transferred into the plasmasphere was found to produce plasmaspheric heating. If this energy is transferred down along the magnetic field lines into the ionosphere, observable ionospheric signatures result during the recovery phase of storms. *Kozyra et al.* [1987] found that the decay of ring current O^+ through Coulomb collisions provides enough energy to produce the subauroral electron temperature enhancement and the associated 6300-Å emission, called a stable auroral red (SAR) arc. The energy loss of ring current ions through Coulomb drag is transferred mainly to the plasmaspheric electrons. Therefore Coulomb collisions cannot be ignored for their important effects on both the energetic and the thermal populations.

In the next section we describe the distribution function and how the number of particles and their energy are calculated by taking moments of the distribution function. In section 3 we present the kinetic equation used for solving the particle drifts and losses. The numerical method used to solve the equation for the distribution function and the boundary conditions are discussed in section 4. In section 5 we describe the model which provides the time variation of the plasmaspheric density, used in calculating the Coulomb interactions. Section 6 explains how the initial conditions of the distribution functions are set up in the model. In section 7 we examine the distribution functions of each of the ion species 12 hours after the main phase of the simulated storm and the buildup of a low-energy population. In section 8 we present the plasmaspheric heating and the corresponding ionospheric signatures. Discussion and summary are given in the final section.

2. Distribution Function

The distribution function used in the present study is defined as:

$$f_s(M,K) \equiv \frac{\delta N_s}{\delta\Phi\, \delta M\, \delta K} \quad (1)$$

Our definition implies that δN_S is the number of particles of

Paper number 93JA01848.
0148-0227/93/93JA-01848$05.00

the species s whose guiding centers are within a flux tube $\delta\Phi$, per increments δM and δK, where Φ is the magnetic flux, M is the first adiabatic invariant and K is a purely field-geometric quantity introduced by *Roederer* [1970]. M and K are defined as

$$M = \frac{E_\perp}{B} = \frac{E\left(1-\mu_o{}^2\right)}{B_o} \tag{2}$$

$$K = \frac{J}{2\sqrt{2m_s M}} = \int_{s_m}^{s'_m}\left[B_m - B(s')\right]^{1/2} ds' \tag{3}$$

where μ_O is the cosine of equatorial pitch angle, B_O is the equatorial magnetic field, m_S is the mass of species s, J is the second adiabatic invariant, B_m is the magnetic field at the mirror points, the integral is evaluated along the field line, and s_m and s'_m are mirror points. The total number of particle of species s is given by

$$N_s = \iiint f_s \, d\Phi \, dM \, dK \tag{4}$$

Given that, $\delta\Phi = B_O \, \delta A_O = B_O \, R_O \, \delta R_O \, \delta\phi$, where δA_O is the equatorial element of area, R_O is the radial distance at the equator, and ϕ is the magnetic local time, we can write

$$N_s = \iiint f_s(t, R_o, \phi, M, K) B_o \, R_o \, dR_o \, d\phi \, dM \, dK \tag{5}$$

In this paper we only consider particles with a pitch angle of 90° (spread δK about K= 0). Therefore the total number of ring current species s, N_S, and the total kinetic energy KE_S, can be written as

$$\begin{aligned} N_s &= \int_0^{\delta K} dK \iiint f_s(t, R_o, \phi, M, K \sim 0) B_o \, R_o \, dR_o \, d\phi \, dM \\ &= c \iiint f_s \, B_o \, R_o \, dR_o \, d\phi \, dM \end{aligned} \tag{6}$$

$$KE_s = c \iiint \frac{1}{2} m_s \mathrm{v}^2 f_s \, B_o \, R_o \, dR_o \, d\phi \, dM \tag{7}$$

c is a normalization constant such that

$$\sum_s KE_s = E_{\text{total}}$$

= total kinetic energy contained in the ring current particles.

There is a simple relation between the phase space distribution function and the distribution function defined in (1). They are proportional to each other and

$$\text{phase space density in (time)}^3\text{(length)}^{-6} = \frac{1}{8\pi}\left(\frac{2m_s^3}{M}\right)^{1/2} f_s \tag{8}$$

3. Drifts and Losses of Ring Current Ions

We define

$$\hat{f}_1(R_o, \phi) = f_s(R_o, \phi, M = M_1, K = K_1) \tag{9}$$

$$\hat{f}_1(R_o, \phi) = \frac{\delta\hat{N}_1}{\delta\Phi} \tag{10}$$

$$\hat{f}_1(R_o, \phi) = \frac{\delta\hat{N}_1}{B_o R_o \delta R_o \delta\phi} \tag{11}$$

Therefore $\delta\hat{N}_1$ is the number of particles per unit M and K about M=M_1 and K=K_1, whose guiding centers are within a flux tube $\delta\Phi$. In the case of no collisions, M is an invariant along the dynamical paths of particles and K is also an invariant if magnetic field lines are equipotential [*Roederer*, 1970]. Therefore $\hat{N}_1$ is a conserved quantity. Assuming a time independent magnetic field, the corresponding conservation equation is

$$\frac{\partial\hat{f}_1}{\partial t} + \frac{1}{B_o R_o}\frac{\partial}{\partial R_o}\left(R_o V_R B_o \hat{f}_1\right) + \frac{1}{R_o}\frac{\partial}{\partial\phi}\left(V_\phi \hat{f}_1\right) = 0 \tag{12}$$

where V_R and V_ϕ are the radial and the longitudinal components, respectively, of the velocity at the reference point 0, for particles with a given $M = M_1$ and $K = K_1$, which have been moving along the flux tube of equatorial cross-section δA_o at point 0. This velocity is usually referred to as the particle's bounce-averaged drift velocity, denoted by $<\mathbf{V_o}>$.

In this work we restrict our study to equatorially mirroring particles, for which K=0 and for which the bounce-averaged drift velocity $<\mathbf{V_o}>$ is just the equatorial drift velocity. In our calculations we assume that the velocity is due to $\mathbf{E} \times \mathbf{B}$ and gradient drifts. A dipolar geomagnetic field is assumed, which is a good assumption for L less than about 6. In this work we are studying the decay of the ring current, which usually takes place inside geostationary orbit ($L \approx 6.6$). The electric field can be expressed as the gradient of a potential, $U(\mathbf{R_o})$, which is the electric potential caused by the convection and the corotation fields. The corotation potential has the form

$$U_{\text{corotation}} = -\frac{C}{R_o} \tag{13}$$

where $C = 1.44\times10^{-2}$ $\mathrm{Vm^{-1}}R_E{}^2$ is a constant. The convection potential can be written as [*Volland*, 1973; *Stern*, 1975]

$$U_{\text{convection}} = aR_o{}^\gamma \sin\phi \tag{14}$$

where ϕ is the magnetic local time with midnight at 0°, a and γ are parameters that characterize the strength of the field and the shielding in the inner magnetosphere respectively. We have used $\gamma = 2$ and a as a function of Kp, given by *Maynard and Chen* [1975] as

$$a = \frac{7.05\times10^{-3}}{\left(1 - 0.159Kp + 0.0093Kp^2\right)^3}\frac{\mathrm{mV/m}}{R_E} \tag{15}$$

where R_E is the radius of the Earth. The radial and longitudinal components of the drift velocity can be written as

$$V_R = -\frac{aR_o{}^{\gamma+2}\cos\phi}{M_E} \tag{16}$$

$$V_\phi = \frac{CR_o + a\gamma R_o{}^{\gamma+2}\sin\phi - 3M_1 M_E/(qR_o)}{M_E} \tag{17}$$

where M_E is the dipole moment of the Earth.

Next we consider the losses of the ring current ions. The loss due to charge exchange with the neutral hydrogen can be described as

$$\left(\frac{\partial f_s}{\partial t}\right)_{ce} = -\mathrm{v}\sigma_s < n_H > f_s \tag{18}$$

where v is the velocity of the particle; σ_S is the cross section for charge exchange of species s with the neutral hydrogen, and $<n_H>$ is the bounce-averaged hydrogen density. Latest measurements of the charge exchange cross section have been

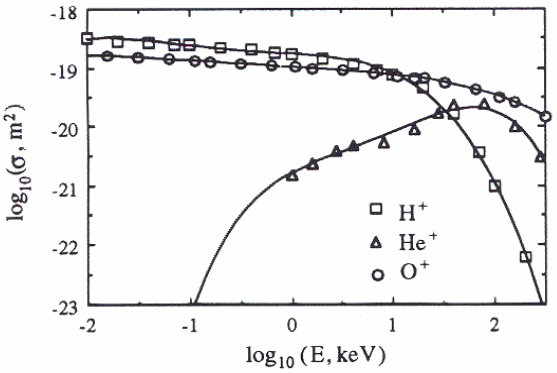

Fig. 1. Charge exchange cross sections of H^+, He^+, and O^+ in hydrogen gas, reported by the Oak Ridge National Laboratory. Solid lines are polynomial fits.

compiled and published by *Phaneuf et al.* [1987] and *Barnett* [1990]. Figure 1 collects all the charge exchange cross-section measurements used in this study and the corresponding polynomial fits. The lowest energy for which there is data available for the cross section of He^+ is at an energy of 1 keV. Below this energy, the values of the cross section may be underestimated by extrapolation of the fit. However, the Coulomb decay lifetime of He^+ at these energies is an order of magnitude shorter than the charge exchange lifetime [*Fok et al.*, 1991*b*]. These low-energy He^+ ions will be removed by Coulomb collisions before they charge exchange with hydrogen atoms. The exospheric hydrogen density, used in our calculations were taken from *Rairden et al.* [1986].

Energetic ring current ions also interact via Coulomb collisions with the thermal particles in the plasmasphere. The ion to electron mass ratio is large, therefore the energy transfer from ring current ions to the thermal electrons in the plasmasphere is significantly more important than angular deflections [*Wentworth et al.*, 1959]. We only consider the changes of M and K of the ring current ions caused by energy losses to thermal plasma in the plasmasphere by the Coulomb drag forces. In fact, K is conserved even with Coulomb drag forces [*Schulz and Lanzerotti*, 1974]. The change of the distribution function by Coulomb drag can be represented by the Fokker-Planck equation, considering only the first-order term,

$$\left(\frac{\partial f_s}{\partial t}\right)_{cc} = -\frac{\partial}{\partial M}\left[\left(\frac{dM}{dt}\right)_{\upsilon} f_s\right] \tag{19}$$

in which the subscript υ refers to frictional process [*Schulz and Lanzerotti*, 1974]. The diffusive terms in the Fokker-Planck equation are neglected. The above equation can be rewritten as

$$\begin{aligned}\left(\frac{\partial f_s}{\partial t}\right)_{cc} &= -\frac{\partial}{\partial M}\left[\left(\frac{\partial M}{\partial E}\right)\left(\frac{dE}{dt}\right)_{\upsilon} f_s\right] \\ &= -\frac{\partial}{\partial M}\left[\frac{M}{E}\left(\frac{dE}{dt}\right)_{\upsilon} f_s\right]\end{aligned} \tag{20}$$

The following expression was obtained by *Spitzer* [1962] for the rate of energy change of a particle moving through a thermal plasma:

$$\frac{dE}{dt} = -\frac{m_s \Gamma_s}{\mathrm{v}} \sum_b < n_b > Z_b^2 \left[2x^2\left(1+\frac{m_s}{m_b}\right)G(x) - erf(x)\right] \tag{21}$$

where

$$x = \frac{\mathrm{v}}{\mathrm{v}_b}$$

$$\Gamma_s = \frac{Z_s{}^2 e^4 \ln \Lambda}{4\pi \varepsilon_o^2 m_s{}^2}$$

s ring current H^+, He^+ or O^+,
b plasmaspheric e^-, H^+, He^+ or O^+,
$\ln \Lambda$ Coulomb logarithm,
$Z_b e$, $Z_s e$ charge of species b and s,
$<n_b>$ bounce-averaged density of plasmaspheric species b,
v_b thermal velocity of b,

$$G(x) = \frac{erf(x) - x\, erf'(x)}{2x^2}$$

$<n_b>$ and $<n_H>$ can be replaced by n_b and n_H respectively for the calculations presented here, because only equatorial mirroring particles were considered. The spatial and temporal variations of the plasmaspheric density n_b were calculated by the model which is described in section 5. The expression for the losses of 90° pitch angle particles, considering charge exchange and Coulomb collision is

$$\begin{aligned}\left(\frac{\partial f_s}{\partial t}\right)_{\text{loss}} &= -\mathrm{v}\sigma_s n_H f_s \\ &+ \frac{\partial}{\partial M}\left\{\frac{2M\Gamma_s}{\mathrm{v}^3}\sum_b n_b Z_b^2\left[2x^2\left(1+\frac{m_s}{m_b}\right)G(x) - erf(x)\right]f_s\right\}\end{aligned} \tag{22}$$

4. Numerical Scheme and Boundary Conditions

The goal of this study was to obtain the time evolution of the distribution function $f_s(t, \mathbf{R}_o, M)$ for a given initial condition, considering both drift and loss. We carried out our calculations using a "two-step" process. In the first step we move particles of different magnetic moments in configuration space, using the drift velocity presented in section 3, over a small time interval, δt. We "reassemble" the distribution function of the particles, and calculate charge exchange loss and Coulomb decay in the next time interval. The method of fractional steps is used to decompose this drift-loss model and only drift or loss is solved at each fractional time step. The algorithm is

$$\hat{f}_i^{\,n+\frac{1}{2}} = \mathfrak{D}(\hat{f}_i^{\,n}) \qquad i = 1,2,3,\cdots \tag{23}$$

where $\hat{f}_i^{\,n}$ is $\hat{f}_i$ at nth time step. The complete distribution function f_s is reassembled

$$f_s^{\,n+\frac{1}{2}} = \sum_i \hat{f}_i^{\,n+\frac{1}{2}} \tag{24}$$

then, losses are calculated.

$$f_s^{n+1} = \mathfrak{L}\left(f_s^{\,n+\frac{1}{2}}\right) \tag{25}$$

$\mathfrak{D} = \mathfrak{D}_R + \mathfrak{D}_\phi$, are the operators for the drift in radial and azimuthal directions. $\mathfrak{L} = \mathfrak{L}_{ce} + \mathfrak{L}_{cc}$ are the operators responsible for the charge exchange loss and Coulomb collisions. The drift and loss operations are reversed on the next time step in order to get second-order accuracy in time.

Different numerical schemes can be applied for different terms. An exact solution can be obtained for the charge

exchange loss term giving

$$\mathcal{L}_{ce} = \exp(-\delta\, t\, v\sigma_s n_H) \tag{26}$$

The Lax-Wendroff scheme together with a flux-limiter method [*LeVeque*, 1992] is used for the linear conservative terms (drifts and Coulomb collisions).

The lower and upper bound in R_o, equatorial radial distance, are taken to be 2 R_E and 6.5 R_E respectively, while the bounds on M correspond to kinetic energy range of 0.01 to 317 keV. The following boundary conditions are applied in this model:

$$f_s(R_o < 2R_E) = 0\ ,\ V_R > 0 \tag{27}$$

$$\left.\frac{\partial f_s}{\partial R_o}\right|_{R_o=6.5R_E} = 0\ ,\ V_R < 0 \tag{28}$$

$$f_s\left(\frac{1}{2}m_s v^2 > 317\ \text{keV}\right) = 0 \tag{29}$$

From (16) we know that V_R is negative on the nightside, therefore the boundary condition (28) for V_R less than zero assumes a continuous injection of ring current at the outer boundary (L=6.5) from the plasma sheet even during the recovery phase of the storm. The rate of this injection depends on the instantaneous particle distribution at the boundary and the strength of the convection electric field. However, this is only a small injection compared with the major injection during the main phase. No lower boundary is needed for energy because Coulomb drag always transports particles toward lower M (energy) in the situation we are considering.

5. The Plasmaspheric Model

In this study the plasmaspheric model of *Rasmussen et al.* [1993] is used to generate numerical values for the parameter $<n_b>$ which appears in (21). We assume that the ions in the plasmasphere have a Maxwellian distribution, with $T_i = T_e =$ 1eV. Plasmaspheric densities are calculated by assuming that there are no sources or sinks of thermal plasma in the equatorial region of the inner magnetosphere. Ion density can change only as a result of ionospheric fluxes or from changes in the volume of a tube of plasma due to magnetospheric convection. The conservation equation used to solve for plasmaspheric density is

$$\frac{\partial <n>}{\partial t} + \frac{dL}{dt}\frac{\partial <n>}{\partial L} + \frac{d\phi}{dt}\frac{\partial <n>}{\partial \phi} = \frac{F_N + F_S}{B_i V} - \frac{<n>}{V}\frac{dL}{dt}\frac{\partial V}{\partial L} \tag{30}$$

where L is the McIlwain parameter, B_i is the magnetic field at the ionosphere, and

$$V(L) = \int \frac{ds}{B} \tag{31}$$

is the volume per unit magnetic flux of a tube of plasma. Note that in this representation, $<n>$ is the average density of H^+ within the tube of plasma. We assume that the He^+ and O^+ densities are 20% and 3% of the H^+ density respectively. The first term on the right-hand side of (30) represents the supply (or loss) of plasma from the conjugate ionospheres and the last term represents the effect of changes in flux tube volume. Changes in volume are calculated by assuming a dipole magnetic field.

Ionospheric fluxes from the northern and southern hemispheres, F_N and F_S, are found by assuming that equilibrium densities are approached at a rate which depends on the deviation from equilibrium and on a constant timescale τ [*Krinberg and Tashchilin*, 1982], i.e.,

$$\frac{F_N + F_S}{B_i V} = \frac{n_o(L,\phi) - <n>(L,\phi)}{\tau} \tag{32}$$

where n_o is the equilibrium density of a completely filled flux tube (obtained from the empirical model of *Carpenter and Anderson* [1992]). The timescale

$$\tau = \frac{n_o B_i V}{F_{N\max} + F_{S\max}} \tag{33}$$

is obtained from (32) by assuming that limiting fluxes are present whenever the flux tube is completely empty ($<n> = 0$). It is at this time that the upgoing ionospheric fluxes are at a maximum, as denoted by the subscripts in (33). These limiting fluxes are calculated from an analytical approximation derived by *Richards and Torr* [1985]. For more information about the plasmaspheric model, see *Rasmussen et al.* [1993].

The plasmaspheric model was run for the main phase and the recovery phase of the model storm. The growth of Kp during the main phase and the decrease of Kp during the recovery phase of ten storms during the period of 1988 to 1990 was averaged, in order to estimate a typical Kp history of a storm (recall that the Kp index is used in the simple model of magnetospheric convection). The maximum Kp is assumed to be 6. Results of the model are shown in Figure 2 for three different times after the main phase of the moderate storm studied in this paper; the modeled time history of Kp of the recovery is also shown in the figure. The post recovery value of Kp is taken to be a constant value of 1. Arrows in Figure 2 indicate the times at which plasmaspheric densities are shown. Magnetospheric convection was strongest at the time corresponding to the plasmaspheric densities shown in Figure 2*a*. The plasmapause is located closer to the Earth (L = 3.5) in the midnight and early morning sectors and a tail of relatively dense plasma can be seen drifting toward the magnetopause in the early afternoon sector. Nine hours later (Figure 2*b*), magnetospheric convection has subsided somewhat and the plasmasphere has begun to refill inside of approximately L = 4 in the post midnight sector. Convection continues to abate and by 27 hours (Figure 2*c*) it has reached a minimum level, predicted by a Kp of 1. During this time period the plasmasphere has continued to refill but has not reached saturated levels. Density contours are nearly circular and density falls off smoothly with L, without an abrupt plasmapause.

6. Initial Conditions of a Moderate Storm

The model calculations presented in this paper assumed that charged particles are accelerated and injected from the plasma sheet on the nightside at the geosynchronous location during the main phase of the storm. These injected particles form the storm time population of the ring current. When recovery starts, the injection which has created the ring current is no longer strong enough to maintain it against the loss processes.

We start our calculations at the end of the main phase when the recovery of the storm begins. The initial storm distributions at zero magnetic local time of the three major ring

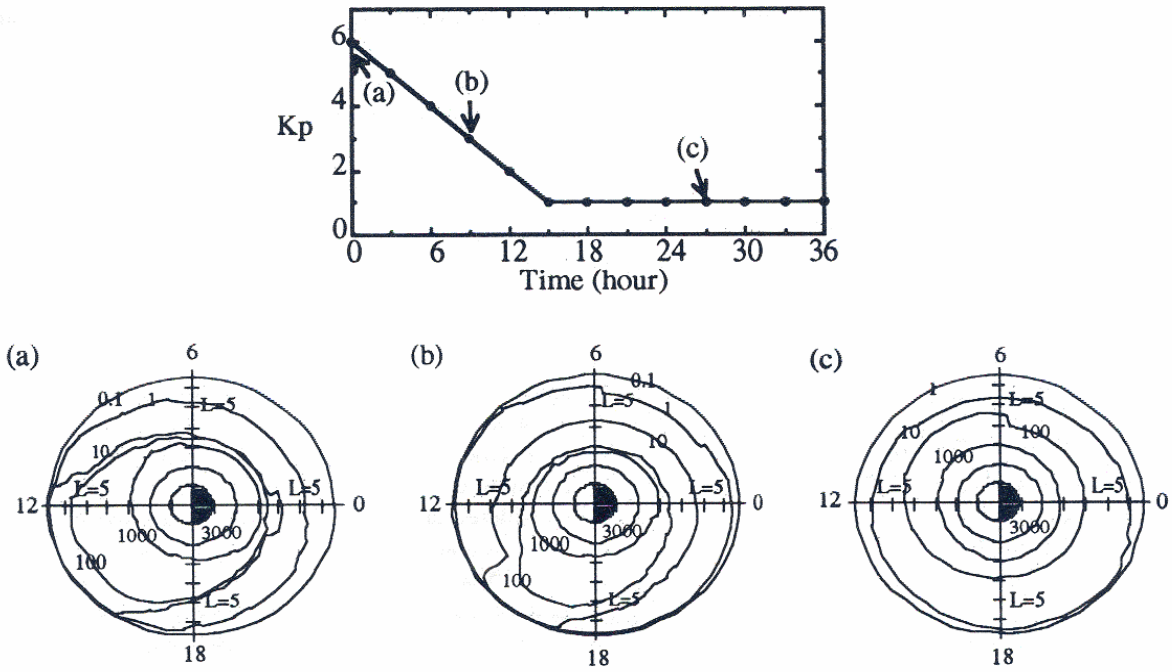

Fig. 2. (Upper panel). Our model for the decay of *Kp* after the main phase of storm. (Lower panel). The modeled plasmaspheric density (in cm^{-3}) during the storm recovery at different times corresponding to the parts a-c indicated in the upper panel.

current ions, H^+, He^+, and O^+ are taken from the average storm time spectra reported by *Kistler et al.* [1989], based on measurements obtained by instruments carried aboard the Active Magnetospheric Particle Tracer Explorers (AMPTE) / Charge Composition Explorer (CCE) spacecraft, during the time period September 1984 to November 1985, which corresponds to solar cycle minimum conditions. They averaged the energy spectra over about 8 moderate storms, with averaged *Kp* of 6, *L* varying from 3.5 to 5.5, in the injection region (between 2000 and 0400 LT). We extrapolate the spectra down to *L* of 2 and up to *L* equal 6.5, using as a guide the radial profile of ring current energy density of the moderate storm on September 4, 1984, reported by *Krimigis et al.* [1985]. For energies less than 1 keV, which were not presented by *Kistler et al.* [1989], the injected distribution functions were estimated by: $f(E) = f(E_o)\, E/E_o\, \exp(1-E/E_o)$, where $E_o = 1$ keV. We decided to make this assumption because it would have been unphysical to chop off the distribution functions at 1 keV and more importantly the buildup of low-energy (< 1 keV) ions due to Coulomb collisions, which will be discussed in section 7, overwhelms this initial population in the plasmasphere as the recovery phase progresses. The variation in the magnitude of the injected distribution function versus local time on the nightside is assumed to be given by a Gaussian, which matches the peak value at midnight and has a standard deviation of 3 hours. This results in a major injection region spanning 2100-0300 MLT. The initial distribution function on the dayside is assumed to be zero. The input spectra for each of the major ion species, at selected *L* values and zero magnetic local time, are shown in Figure 3. The distribution functions plotted in all figures presented in this paper are phase space distribution functions given in s^3/km^6.

The total kinetic energy (E_{total}) of the ring current particles injected during the main phase of the storm is assumed to be 2.0×10^{31} keV. The initial percentages of the total energy and the number density provided by each ion species, averaged over *L* values from 2 to 6.5, is shown in Figure 4*a* [*Kistler et al.*, 1989]. The initial mean energy of each species, as a function of *L*, is shown in Figure 4*b*. H^+ provided the major portion of

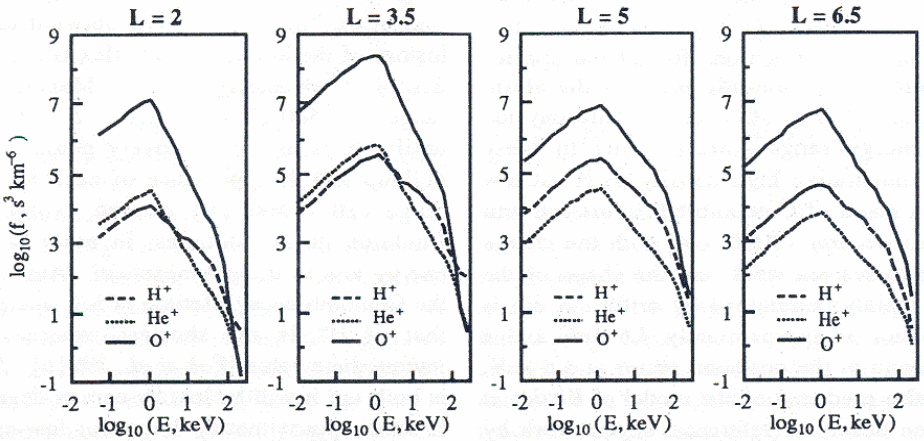

Fig. 3. "Initial" conditions on the phase-space density of H^+, He^+, and O^+ at different *L* values, magnetic midnight.

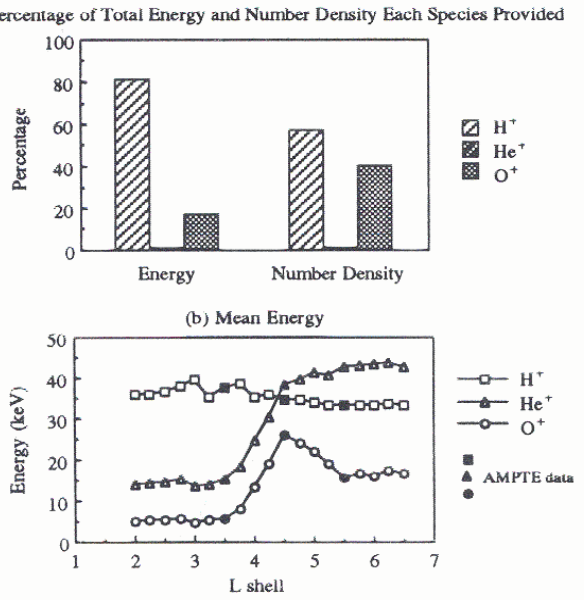

Fig. 4. Characteristics of the ring current ion population just before the recovery phase of storm. (*a*) Percentage of total energy and number density each species provided; (*b*) Mean energy. Inputs are taken from *Kistler et al.* [1989].

the total energy while He^+ provided only a small percentage of the total energy and number density. The initial mean energy of the ring current H^+ is quite constant over the L-shell range of the observations. The initial mean energies of He^+ and O^+ are low at low L and are higher at $L > 4.5$.

7. Change of Energy Spectra and Buildup of Low Energy Population

The phase space distribution functions of all ion species after 12 hours of decay are plotted in Figure 5; the results are presented as a function of energy at L = 2.5, 4 and 5.5, and at selected local times centered in the nightside, prenoon and postnoon sectors. At L = 2.5 there are sharp decreases in the distribution function at energies between 10 and 20 keV in both the prenoon and postnoon sectors. This kind of drop off in the distribution function is a consequence of the combined effects of the corotation and convection electric fields and gradients in the magnetic field on the ion drift. Corotation, which produces eastward drifts, dominates the motion of low-energy ions (E < 5 keV), whereas high-energy ions (E > 30 keV) drift westward due to the gradient in the magnetic field. In both cases the drift paths are closed. At some intermediate energy the corotation and convection drifts almost cancel the gradient drift, resulting in very slow drift velocities. Particles at these energies take days to reach the dayside. As stated in section 6, the initial distribution functions for all ion species were assumed to be zero on the dayside prior to the storm injection. Therefore a sharp drop off occurs in the dayside distribution over the energy range corresponding to these stagnating ions. The comparative high density in H^+ at low energies (< 500 eV) is a result of Coulomb collisions and will be discussed later in this section. At L = 4, both the charge exchange and Coulomb losses are weak and the shape of the distribution function is mainly determined by drifts. A dip is seen in the prenoon sector at approximately 7.6 keV and a sharp drop off can be found in the postnoon sector at 3.8 keV. These two features are also predicted by the model of *Kistler et al.* [1989] and have been observed (references in the work by *Kistler et al.* [1989]). At L = 5.5 the distribution functions are quite symmetric about local time, although there is still a postnoon drop off.

In order to separate the effects of drifts, charge exchange and Coulomb drag, the model was run again for two test cases: (1) considering only drift motion and (2) drifts plus only charge exchange loss. Figure 6 shows these test results of H^+ at three locations. At L=2.5, the inclusion of Coulomb collisions results in a slight reduction of the distribution function at high energies. However, a low-energy (< 500 eV) ion population is formed by the energy degradation of high-energy ions due to Coulomb collisions with the plasmaspheric electrons. Coulomb collisions also make the dips caused by drift motion shallower. This increase in the ion distribution due to Coulomb collisions was also found by *Cornwall* [1972] and *Spjeldvik* [1977], when they calculated the equilibrium density structure of the magnetospheric ions. *Kistler et al.* [1989] only considered drifts and charge exchange loss of ring current ions. They found that at low energies, the observed spectra were higher than predicted and that the dips in some of their modeled spectra was deeper than the measurements. The inclusion of Coulomb collisions in our model leads to a better agreement with observations, especially at low energies. Coulomb drag also has pronounced effects on the low energy distribution of ring current He^+ and O^+ ions. At L values outside the plasmapause (L=4 and 5.5) the Coulomb collision effects are relatively much weaker.

The low-energy ion population in the magnetosphere has been studied by in-situ satellite measurements [*Lennartsson and Reasoner*, 1978; *Lennartsson and Sharp*, 1982]. We calculate the 10 - 500 eV flux derived from each ring current ion species as a function of elapsed time. Plate 1 shows the initial flux, and the flux at 12 hours and 2 days after the main phase of the storm. For all ions the maximum flux is initially located in the region of L between 3 and 4 (Plate 1*a*). 12 hours later (Plate 1*b*), flux of the same order of magnitude or higher than the initial peak is found at a lower L shell (L ~ 2.5). A close look at the drift paths of these low-energy particles indicates that the build-up of the low-energy population at lower L value is not a consequence of the drift of these particles from higher L to this location, but is the result of energy degradation of higher-energy ring current ions by Coulomb collisions with the plasmasphere. We also found, as shown in Plate 1, that particles at L values above about 4, which have open drift paths, drift toward the upper spatial boundary of the model and are lost; therefore the longest-lived fluxes are confined to a range of L values from approximately 2.5 to 3.5.

After 2 days of recovery (Plate 1*c*), there is an order of magnitude decrease in the maximum H^+ flux. The maximum flux at this time has moved outward to L ~ 4. The temporal history of the low-energy O^+ flux is much different than the just described low-energy H^+ ions. Maximum O^+ flux in the energy range 10 - 500 eV is located at L ~ 2.75, but does not appear until 2 days into the recovery phase. The different times for buildup and disappearance of each ion species in this energy range (10 - 500 eV) can be explained by their different Coulomb decay lifetimes; in other words, by their rates of energy loss to the plasmasphere. Among the three ion species, the Coulomb decay lifetime of low-energy O^+ is the longest and that of H^+ is the shortest, whereas that of He^+ has an intermediate value [*Fok et al.*, 1991*b*]. After the low-energy H^+ is built up, it will be lost by energy degradation in a few hours. It takes approximately 1 day for low-energy O^+ to be formed from high-energy particles, as a result of its comparatively

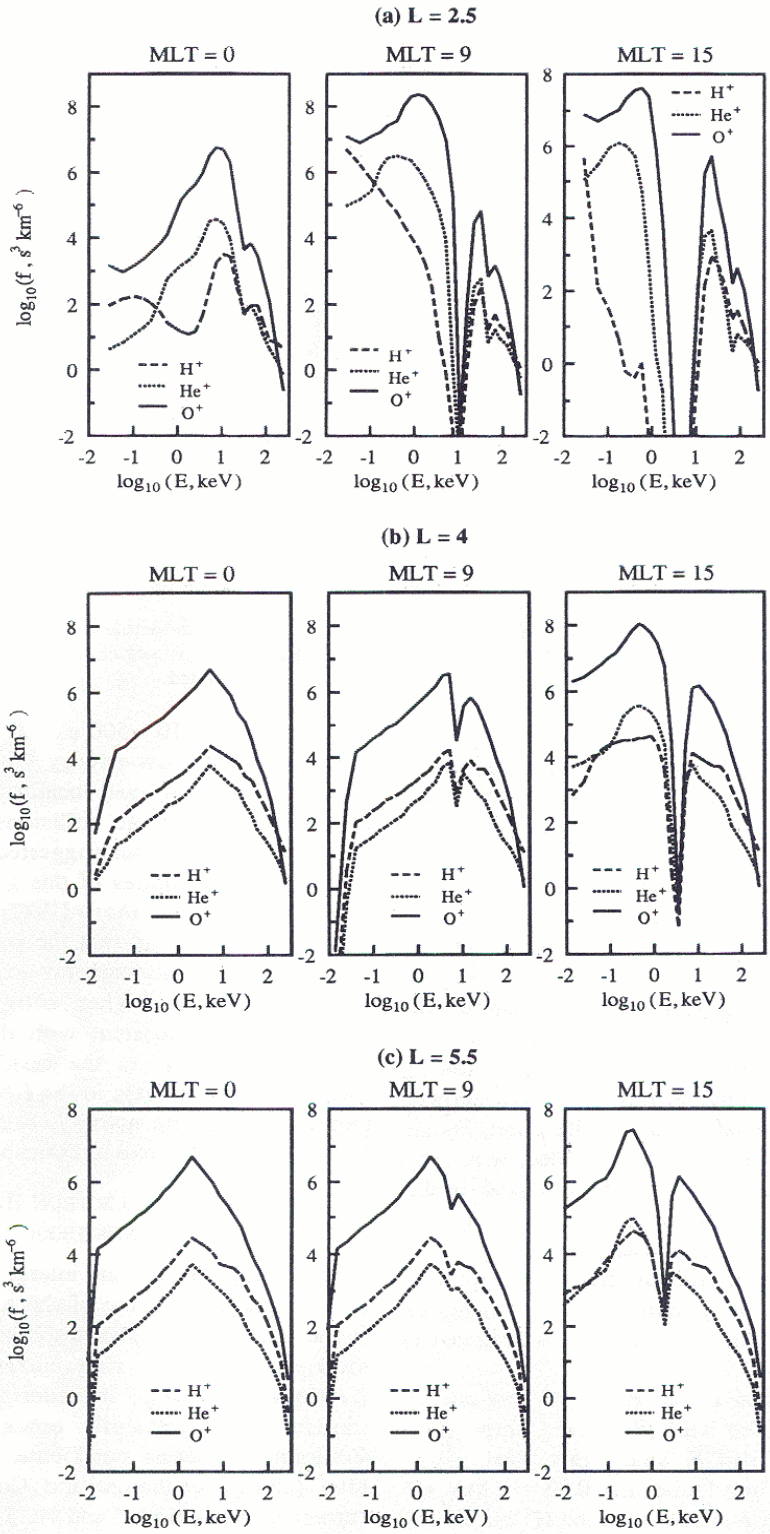

Fig. 5. Phase space distribution functions of major ring current ions at different L shells and different magnetic local times, 12 hours after the moderate storm main phase: (*a*) $L = 2.5$; (*b*) $L = 4$; (*c*) $L = 5.5$.

long Coulomb lifetime, and therefore it lasts for a few days.

The effects of Coulomb drag on the ion distribution are clearly illustrated in Figure 7. The ring current model was run, excluding drifts and charge exchange loss, for a number of simplified energetic ion distributions, to isolate the effects of Coulomb drag on the temporal evolution of these distributions. The simulation begins at t=0 with initial H^+ (Figure 7*a*) and O^+ (Figure 7*b*) ion distributions peaking at 10 keV (top panel) and 40 keV (middle panel) in a background thermal (1 eV) plasma with density of 2000 cm^{-3}. The variation in rate of energy loss as a function of ion energy (bottom panel) is provided as a convenient reference. Ions move from high to low energy at a rate, given in the bottom panels of Figure 7*a* and 7*b*, which is a function of location in energy space. Energy loss rate in energy space peaks at 4 keV for H^+ (bottom panel, Figure 7*a*) and at 50 keV for O^+ (bottom panel, Figure 7*b*). Ions will be removed rapidly from regions of peak energy loss rate and will buildup in regions of lower-energy loss rate. The effect is

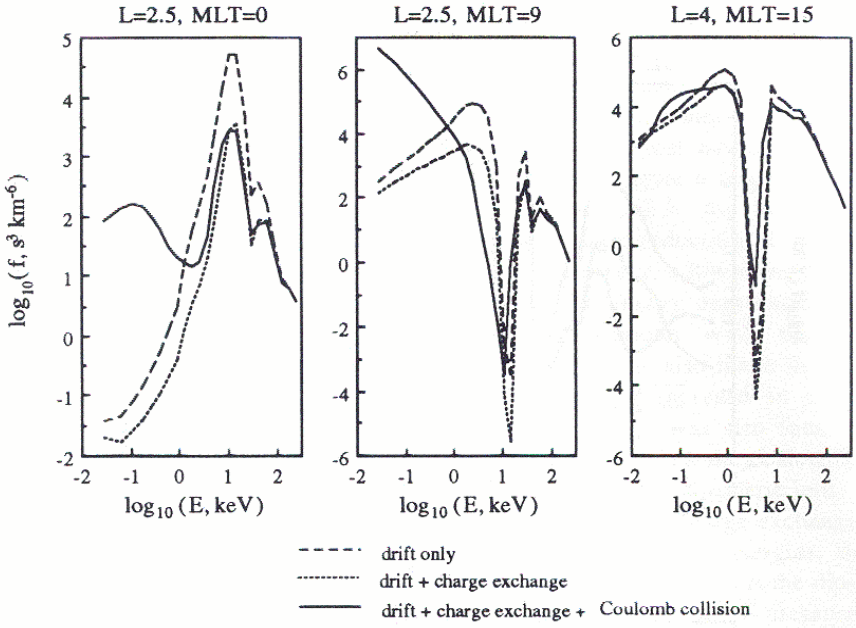

Fig. 6. Phase space distribution functions of ring current H^+ at 12 hours after the moderate storm main phase. Dashed lines represent results when only drift is considered. Dotted lines contain effects of drift and charge exchange, while solid lines represent results under the same conditions except Coulomb collisions are also included.

dramatically illustrated in the top panels of Figure 7*a* and 7*b*. A low-energy (< 500 eV) flux of H^+ builds up after 12 hours, as a result of energy loss by the "10 keV" H^+. However, this low-energy population diminishes after 2 days of decay, consistent with the results of model calculations presented earlier. Low-energy O^+ fluxes builds up more slowly. They only reach values comparable to the peak low-energy H^+ fluxes after 2 days have elapsed. In contrast the peak low-energy H^+ fluxes appear after 1 day of decay.

The buildup of low-energy ions from a 40-keV initial ion distribution is much less dramatic (middle panels, Figure 7*a* and 7*b*). The 40-keV peak in the H^+ flux occurs in a region of increasing energy loss rate. Ions move from a region of slower to faster energy loss (toward the left in the middle panel, Figure 7a). As a consequence, the H^+ distribution is eroded, with only a weak buildup at the lowest energies. The 40-keV peak in the O^+ flux (middle panel, Figure 7b), occurs in a region of nearly constant energy loss rate. For this case the O^+ peak is convected in energy space, almost without change in amplitude or shape, to lower energies. Eventually, as time increases beyond 2 days, a flux buildup at the low energies is expected to occur.

Shelley et al. [1985] reported observations of low-energy plasma (< 17 keV) from the Hot Plasma Composition Experiment on the AMPTE/CCE spacecraft during the September 4, 1984, storm. They found that 0.03 - 1 keV O^+ extended to significantly lower L values than the H^+ during the storm recovery, which is consistent with results from our ring current model (Plate 1). The maximum flux level we obtained is of the order of 10^6 $cm^{-2}s^{-1}$, which corresponds to a number density of approximately 1 cm^{-3}. This is also in agreement with ISEE 1 observations reported by *Lennartsson and Sharp* [1982] and *Shelley et al.* [1985].

Low-energy ion populations at $L \sim 2$-3 have been observed in the past but their source was not clear. Injection from the tail along the plasma sheet and consequent penetration into the plasmasphere was suggested as a possible source [*Newell and Meng*, 1986]. However, very seldom are electric fields strong enough to move particles from the tail deep down to $L \sim 2$-3 with energies of 10 - 500 eV at this location. We suggest that the enhanced low-energy ion population, within the plasmasphere, is formed locally from high-energy ring current particles, via Coulomb collisions with the thermal plasma in the plasmasphere. Our suggested mechanism can also explain some observed features of this low-energy population reported by *Lennartsson and Sharp* [1982]. They found that O^+ was the dominant species and that the position of the low-energy ions was a function of magnetic activity, with smaller L values corresponding to higher activity. Our proposed source mechanism is consistent with these observed features. The dominance of O^+ is the result of the different Coulomb lifetimes. The decrease in the L value of the plasmapause, with increased magnetic activity, causes the region of significant Coulomb drag to move to correspondingly lower L values.

8. Plasmaspheric Electron Heating and the Associated Ionospheric Signatures

When ring current ions interact via Coulomb collisions with the plasmasphere, some of the energy of the ring current ions is transferred to the plasmaspheric electrons. We calculate the total energy of the ring current ions, using (7), at every fractional time step, in order to obtain the rate of energy transfer for a particular process. Our model shows that Coulomb collisions contribute a significant fraction of the total (charge exchange and Coulomb) energy loss of ring current heavy ions (O^+ and He^+) in the plasmasphere region ($L \leq 3$) in this particular storm. For example, at $L = 2.5$ the percentage of the total O^+ energy loss due to Coulomb drag is 22% and that for He^+ is 54%. The energy transferred from ring current ions to the plasmasphere has a significant effect on the thermal plasma in the plasmasphere. The transport of this plasmaspheric heat flux down to the ionosphere along field lines, has been proposed as the energy source of the subauroral electron temperature enhancement and the associated SAR arc [*Cole*, 1965; *Kozyra et al.*, 1987]. *Kozyra et al.* [1987] also showed that ring current O^+ ions, with energies of tens of keV, provide the major portion of this plasmaspheric-ionospheric heat source.

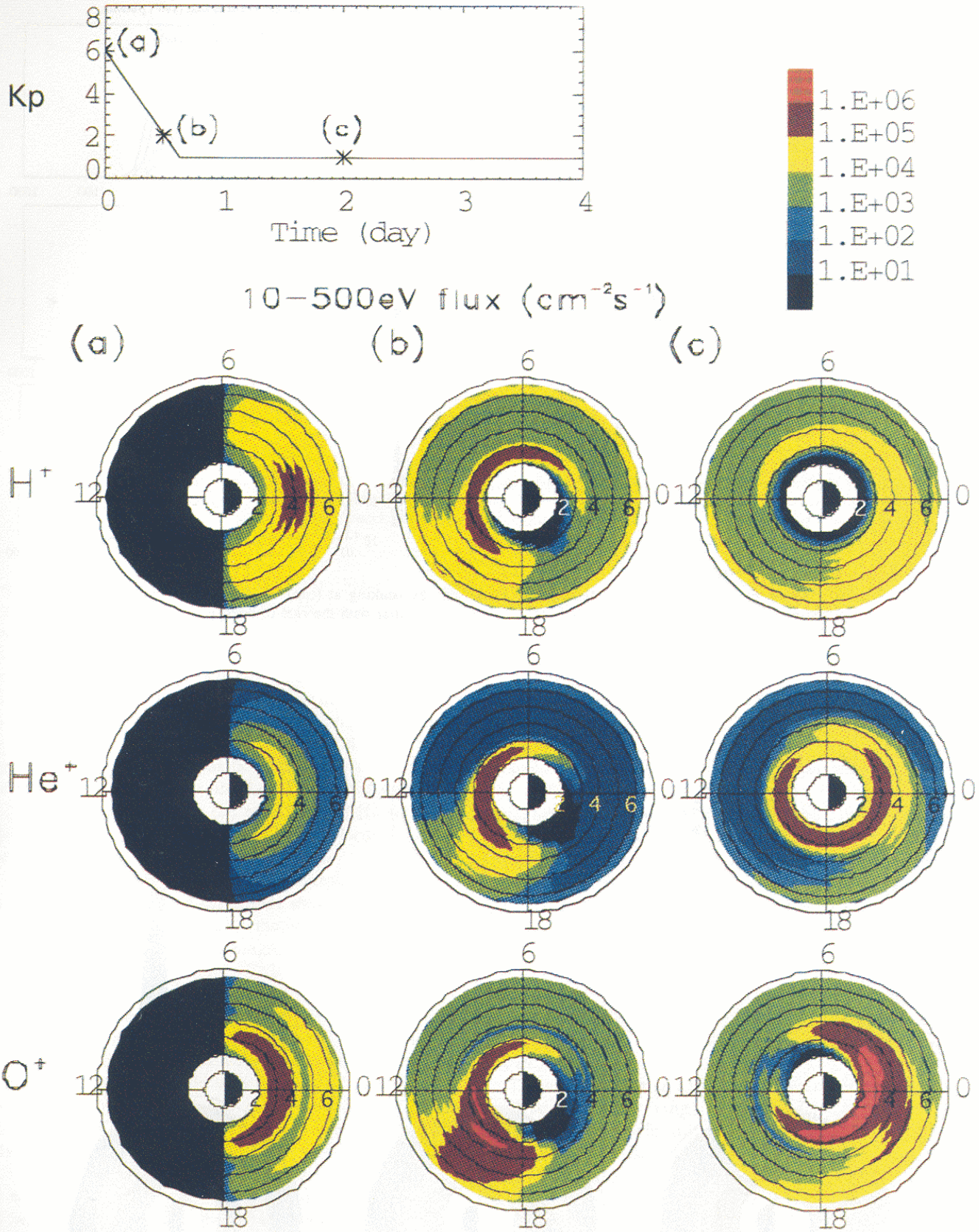

Plate 1. (Upper panel:) Model decay of *Kp* after the main phase of storm. (Lower panel) 10-500 eV ion flux in $cm^{-2}s^{-1}$ at different times of the recovery phase of the storm: (*a*) 0 hour, (*b*) 12 hours, and (*c*) 2 days.

Our model results show that O^+ is always the major contributor to plasmaspheric electron heating. Plate 2 shows the energy-deposition rate at different times during the recovery phase of the storm. At 1 hour after the storm main phase, the maximum energy-deposition is of the order of 10^9 eV cm^{-2} s^{-1} and is located on the nightside at $L \sim 3$, the location of the maximum in the initial injected population. The shape of the energy-deposition contours corresponds, in general, to the shape of the contours of plasmaspheric density (Figure 2*a*), because the energy deposition rate is proportional

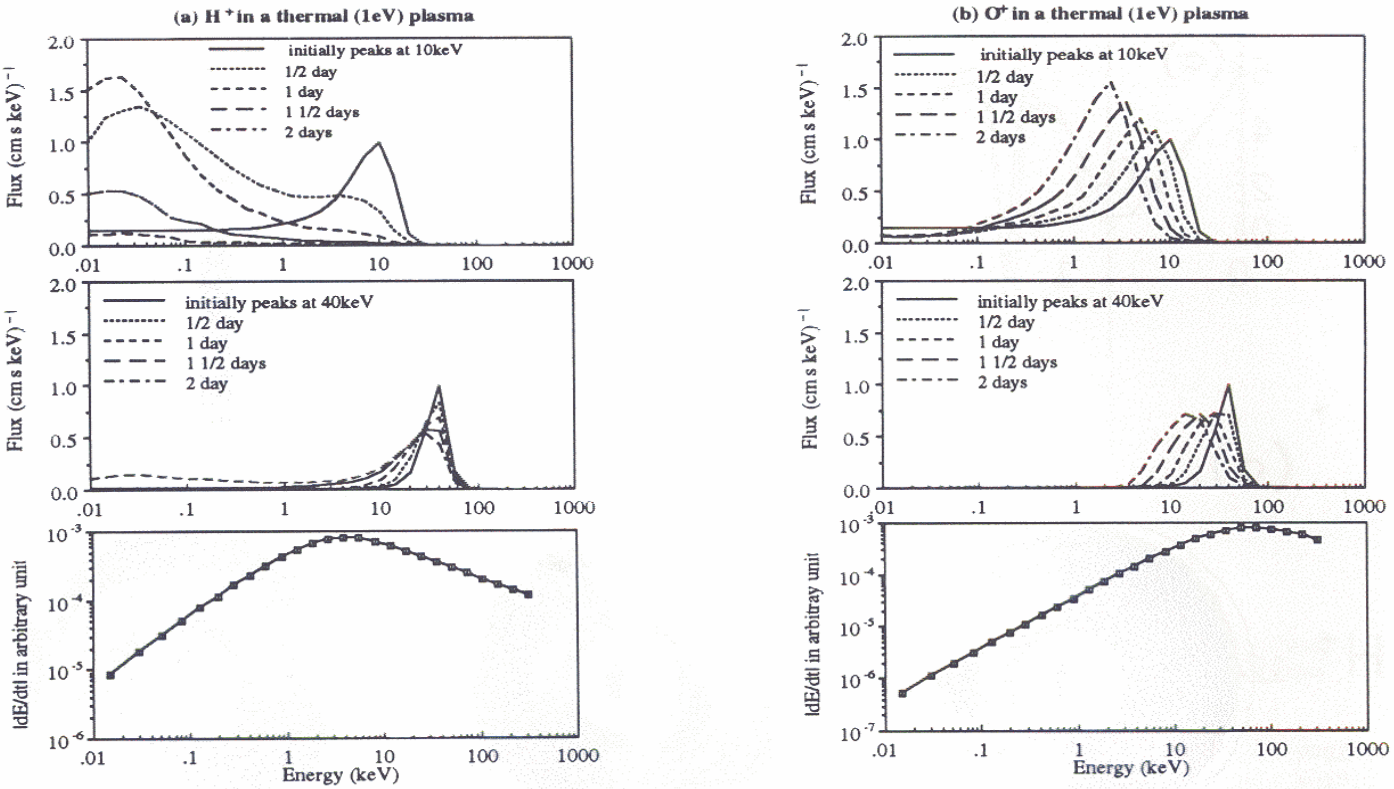

Fig. 7. Time variations of (*a*) H^+ and (*b*) O^+ fluxes with initial energy peaking at (top) 10 keV and (middle) 40 keV in a background of thermal plasma (1 eV, density = 2000 cm^{-3}), (bottom) together with the rate of energy loss as a function of ion energy.

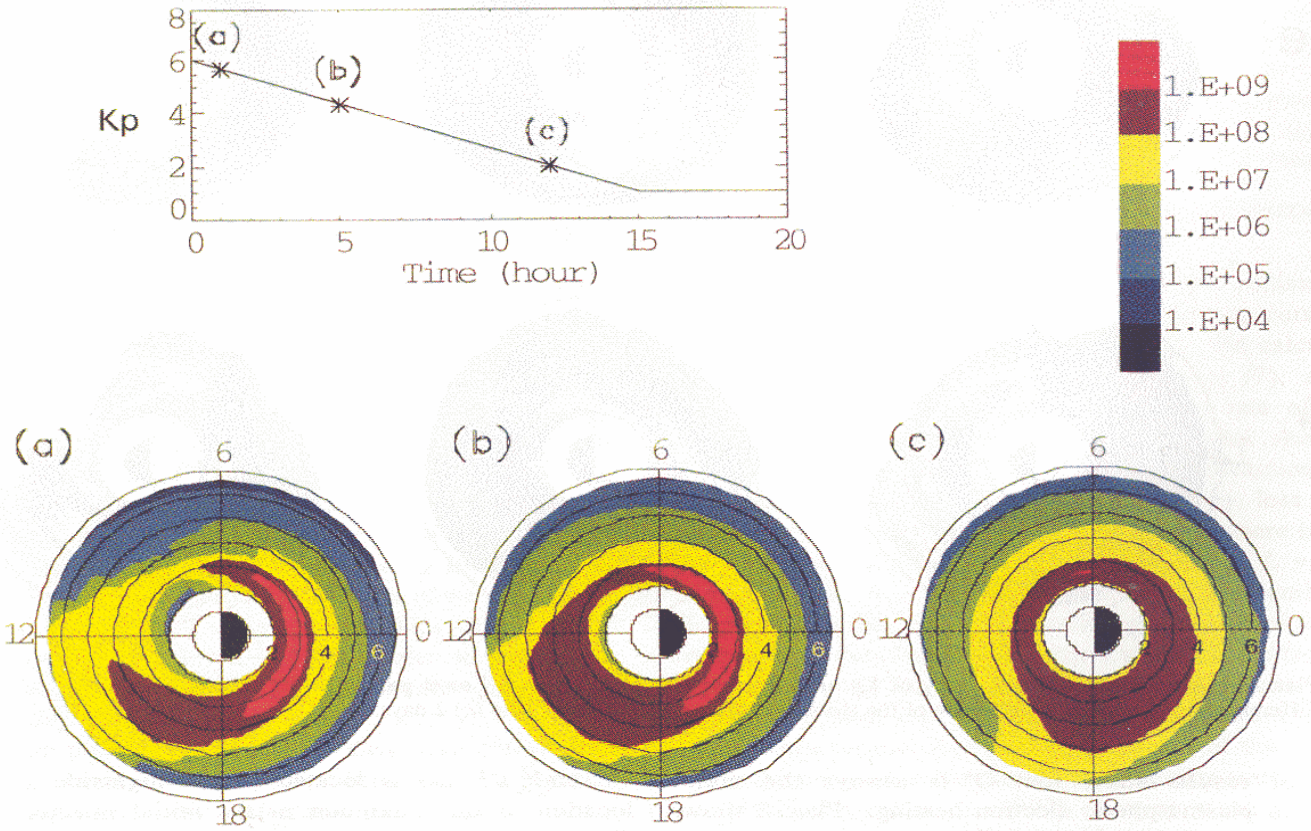

Plate 2. (Upper panel) Model decay of *Kp* after the main phase of storm. (Lower panel) Energy deposition rate in eV cm^{-2} s^{-1} to plasmaspheric electrons at three elapsed times of the recovery phase of the storm indicated in the upper panel, that is (a) 1 hour, (*b*) 5 hours, and (*c*) 12 hours.

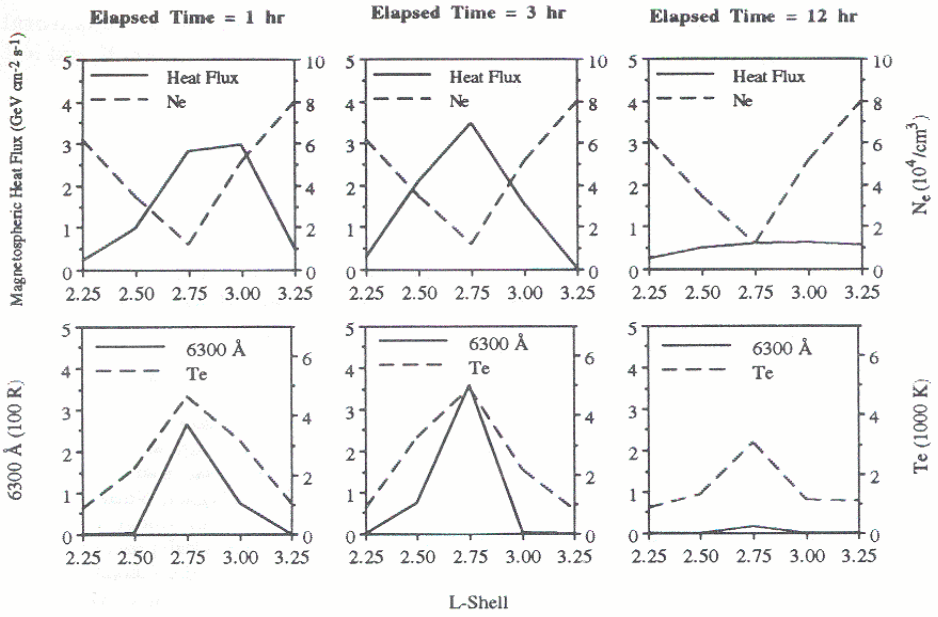

Fig. 8. The ionospheric responses of the plasmaspheric heating at different elapsed times during the recovery phase of the storm. (Upper panel) Magnetospheric heat flux at midnight, L from 2.25 to 3.25, and the ionospheric electron density at 400 km at the same local time and L shells. (Lower panel:) 6300-Å emission and electron temperature at the same time and position of electron density.

to the plasmaspheric density ($<n_b>$ in (21)). Four hours later the region of significant energy transfer moves in a westward direction and extends further to the postnoon sector (Plate 2*b*). This movement of the region of significant energy transfer is consistent with the proposal that O^+ ions in the energy range of tens of keV (which drift westward) are the main source of this energy. A bulge in the region over which energy is deposited can also be seen on the duskside, as a result of the well known plasmaspheric bulge. The deposition rate starts to decrease at approximately 12 hours after the beginning of the recovery phase (Plate 2*c*). At this time the region of significant energy deposition is more symmetric about magnetic local time when compared to that earlier in the recovery phase.

The consequences to the subauroral ionosphere of electron energy deposition rates of the magnitude shown in Plate 2 were next examined. A cross section of the energy deposition rate contours was taken at midnight magnetic local time at each time step during the simulation. This procedure provides a temporally varying energy deposition rate versus L value at 24 MLT during the storm simulation. The energy deposited in the electron gas is assumed to be transported along field lines into the magnetically connected subauroral ionosphere as a heat flux. This assumption is valid only if the electrons inside the plasmasphere are collisional. For a collisional description of the plasma to be valid, the electron-electron collision time must be less than the electron bounce time [*Cornwall et al.*, 1971]. This condition is just satisfied for the plasmaspheric model we used in this study. A one-dimensional ionosphere model with upper boundary heat flux supplied by the ring current drift-loss model was solved at discrete L values across the midnight ionosphere. The ionosphere model was originally developed by *Young et al.* [1980] and was described in some detail by *Kozyra et al.* [1990]. The neutral atmosphere was specified by the MSIS-86 model [*Hedin*, 1987] for fall solar minimum conditions. An IRI-86 model [*Bilitza*, 1986] ionospheric profile was assumed but was scaled to represent the main ionospheric density trough. The ionospheric electron density trough is a persistent large-scale feature of the nightside subauroral region [*Best and Wagner*, 1983]. Observations of 1000 troughs by ARIEL III indicate that the trough occurrence frequency increases with increasing geomagnetic activity [*Tulunay and Sayers*, 1971]. We took a typical nightside ionospheric N_e trough from the measurements made by the AE-C satellite in 1974, during solar cycle minimum, at $Kp \sim 6$. The electron density was assumed to be constant with time during the storm recovery. The upper panel of Figure 8 shows a latitudinal profile of the model inputs at different times during the storm recovery: the magnetospheric heat flux obtained from our drift-loss model and the ionospheric electron density at 400 km altitude. We calculate the corresponding T_e value at 400 km and the column 6300 Å emission rates; the results of these calculations are plotted in the lower panel of Figure 8. The peak values of the calculated red line intensities are in the 200 to 400 R range during the early phase of the recovery, consistent with the observed values during moderate storms at solar cycle minimum [*Slater and Kleckner*, 1989]. The calculated peak values in the electron temperature of 4000 - 6000 K during the early phase of the recovery are also consistent with the observed values [*Fok et al.*, 1991*a*].

The energy transferred to the plasmasphere through Coulomb collisions with ring current ions is mainly to the plasmaspheric electron population [*Fok et al.*, 1991*b*]. However, since the conductivity of ions is only one fortieth of that of electrons, small amounts of energy transferred to plasmaspheric ions may have a significant effect on the plasmaspheric ion temperature. The reduced conductivities of ions compared to electrons implies that energy will be transported away from the equatorial region more slowly in the ion gas than in the electron gas; thus a smaller heat source is required to maintain significant temperatures in the ion than in the electron plasmaspheric populations. We calculated the energy transfer of ring current ions to the plasmaspheric ions. The maximum energy-deposition rate was found to be of the order of 10^8 eV cm^{-2} s^{-1}, which is about an order of magnitude lower than that for the electron. We estimated the

corresponding plasmaspheric ion temperature and found that it is approximately 4000 K at L=2.75, on the nightside, thus this seemingly small energy deposition rate does have an important impact on the nightside ion temperatures.

9. Discussion and Summary

In many studies of ring current or trapped particle interactions, only charge exchange with neutrals and wave-particle interactions have been considered; Coulomb collisions between ring current ions and the plasmasphere have been neglected [cf. *Kistler et al.*, 1989; *Roelof and Williams*, 1988; *Williams et al.*, 1973]. *Cole* [1965] and *Kozyra et al.* [1987] found that Coulomb collisions between ring current ions and thermal electrons have significant effects on the plasmasphere and thus on the formation of such ionospheric phenomena as the subauroral electron temperature enhancements and SAR arcs. Nevertheless, the effects of Coulomb collisions on the ring current population itself, as a function of the elapsed time during the recovery phase of storms, have not been addressed. *Fok et al.* [1991*b*] obtained an improved expression for the ring current Coulomb decay lifetime in the presence of a thermal plasma. They found that Coulomb lifetimes are comparable with charge exchange lifetimes for ring current major ions below a few tens of keV. In this work we have shown that including Coulomb collisions in the calculation of ring current ion behavior leads to better agreement between calculated and observed features, especially at low energies. Furthermore, we found that Coulomb collisions result in the appearance of low energy (< 500 eV) ions. Ion populations with similar characteristics have been observed previously in the ring current region, but their origin has not been established. Our work has demonstrated that Coulomb collisions between ring current ions and the plasmasphere are important and need to be considered.

SAR arcs have been observed and studied for many years. SAR arcs emissions are relatively long lived compared with the rapidly changing poleward auroral phenomena. It has not been possible to "follow" red arcs after dawn, because of overwhelming day glow intensities. Our study found that the SAR arc energy source is present on the dayside (see Plate 2*b*) although the predicted intensity is too weak to be detectable by ground-based photometers over the day glow. We also found that the plasmaspheric heating and related electron temperature enhancements and emissions, fade away in approximately 10 hours, for the particular storm that we modeled.

In summary, our drift-loss model allowed us to obtain the time evolution of the distribution functions of the three major ring current ion species (H^+, He^+, and O^+) during the recovery phase of a model storm of moderate intensity. We found that

1. Coulomb collisions increase the ion densities at energies below 1 keV and make the dips in phase-space density, caused by drift motions and charge exchange loss, shallower.

2. A buildup of low-energy (< 500 eV) ions is found inside the plasmapause (as a result of energy degradation of the ring current ions caused by Coulomb collisions with the plasmasphere), with O^+ being the dominant species of this population.

3. The energy transferred from the ring current ions to the plasmaspheric electrons via Coulomb collisions provides a significant energy source to power the subauroral electron temperature enhancements and the associated SAR arcs. The maximum energy-deposition rate is of the order of 10^9 eV cm^{-2} s^{-1}, which produces a subauroral electron temperature enhancement of 4000 - 6000 K and a SAR arc intensity of 200 - 400 R.

4. The peak energy transfer from the ring current ions to the plasmaspheric ions is of the order of 10^8 eV cm^{-2} s^{-1}, and the estimated nightside ion temperature is 4000 K at L=2.75.

Acknowledgments. We wish to thank NASA for support under grant numbers NAGW-1619 and NAG5-1542 and NSF for support under grant number ATM-9114409 and ATM-9116858.

The Editor thanks M. Schulz and another referee for their assistance in evaluating this paper.

References

Barnett, C. F., Atomic data for fusion, vol. I, Collisions of H, H_2, He and Li atoms and Ions with atoms and molecules, *Tech. Rep. ORNL-6086/V1*, Oak Ridge Nat. Lab., Oak Ridge, Tenn., 1990.

Best, A., and C.-U. Wagner, Variations of electron density and electron temperature in the main trough of the ionosphere, paper presented at the symposium: Physical processes in the main ionospheric trough region, organized by The Geophysical Institute of the Czechoslovak Academy of Sciences, Prague, March 1983.

Bilitza, D., International reference ionosphere: Recent developments, *Radio Sci., 21*, 343-346, 1986.

Carpenter, D. L., and R. R. Anderson, An ISEE/Whistler model of equatorial electron density in the magnetosphere, *J. Geophys. Res., 97*, 1097-1108, 1992.

Chen M. W., M. Schulz, L. R. Lyons, and D. J. Gorney, Stormtime transport of ring current and radiation belt ions, *J. Geophys. Res., 98*, 3835-3849, 1993.

Cole, K. D., Stable auroral red arc, sinks for energy of Dst main phase, *J. Geophys. Res., 70*, 1689-1706, 1965.

Cornwall, J. M., Radial diffusion of ionized helium and protons: a probe for magnetospheric dynamics, *J. Geophys. Res., 77*, 1756-1770, 1972.

Cornwall, J. M., F. V. Coroniti, and R. M. Thorne, Unified theory of SAR arc formation at the plasmasphere, *J. Geophys. Res., 76*, 4428-4445, 1971.

Fok, M.-C., J. U. Kozyra, and L. H. Brace, Solar cycle variation in the subauroral electron temperature enhancement: Comparison of AE-C and DE 2 satellite observations, *J. Geophys. Res., 96*, 1861-1866, 1991*a*.

Fok, M.-C., J. U. Kozyra, A. F. Nagy, and T. E. Cravens, Lifetime of ring current particles due to Coulomb collisions in the plasmasphere, *J. Geophys. Res, 96*, 7861-7867, 1991*b*.

Hedin, A. E., MSIS-86 thermospheric model, *J. Geophys. Res., 92*, 4649-4662, 1987.

Kistler, L. M., F. M. Ipavich, D. C. Hamilton, G. Gloeckler, B. Wilken, G. Kremser, and W. Stüdemann, Energy spectra of the major ion species in the ring current during geomagnetic storms, *J. Geophys. Res., 94*, 3579-3599, 1989.

Kozyra, J. U., E. G. Shelley, R. H. Comfort, L. H. Brace, T. E. Cravens, and A. F. Nagy, The role of ring current O^+ in the formation of stable auroral red arcs, *J. Geophys. Res., 92*, 7487-7502, 1987.

Kozyra, J. U., C. E. Valladares, H. C. Carlson, M. J. Buonsanto, and D. W. Slater, A theoretical study of the seasonal and solar cycle variations of stable aurora red arcs, *J. Geophys. Res., 95*, 12,219-12,234, 1990.

Krimigis, S. M., G. Gloeckler, R. W. McEntire, T. A. Potemra, F. L. Scarf, and E. G. Shelley, Magnetic storm of September 4, 1984: A synthesis of ring current spectra and energy densities measured with AMPTE/CCE, *Geophys. Res. Lett., 12*, 329-332, 1985.

Krinberg, I. A., and A. V. Tashchilin, Refilling of geomagnetic force tubes with a thermal plasma after magnetic disturbance, *Ann. Geophys., 38*, 25-32, 1982.

Lennartsson, W., and D. L. Reasoner, Low-energy plasma observations at synchronous orbit, *J. Geophys. Res., 83*, 2145-2156, 1978.

Lennartsson, W., and R. D. Sharp, A comparison of the 0.1-17 keV/e ion composition in the near equatorial magnetosphere between quiet and disturbed conditions, *J. Geophys. Res., 87*, 6109-6120, 1982.

LeVeque, R. J., *Numerical Methods for Conservation Laws*, 2nd ed., chap. 16, Birkhäuser Verlag, Boston, Mass., 1992.

Maynard, N. C., and A. J. Chen, Isolated cold plasma regions: Observations and their relation to possible production mechanisms, *J. Geophys. Res., 80*, 1009-1013, 1975.

Newell, P. T., and C.-I. Meng, Substorm introduction of ≤ 1-keV magnetospheric ions into the inner plasmasphere, *J. Geophys. Res., 91*,

11,133-11,145, 1986.

Phaneuf, R. A., R. K. Janev, and M. S. Pindzola, Atomic data for Fusion, vol. V, Collisions of Carbon and Oxygen Ions with Electrons, H, H_2 and He, *Tech. Rep. ORNL-6090/V5*, Oak Ridge Nat. Lab., Oak Ridge, Tenn., 1987.

Rairden, R. L., L. A. Frank, and J. D. Craven, Geocoronal imaging with Dynamics Explorer, *J. Geophys. Res., 91*, 13,613-13,630, 1986.

Rasmussen, C. E., S. M. Guiter, and S. G. Thomas, Two-dimensional model of the plasmasphere: refilling time constants, *Planet. Space Sci., 41*, 35, 1993.

Richards, P. G., and D. G. Torr, Seasonal, diurnal, and solar cyclical variations of the limiting H^+ flux in the Earth's topside ionosphere, *J. Geophys. Res., 90*, 5261-5268, 1985.

Roederer, J. G., *Dynamics of Geomagnetically Trapped Radiation*, chap. 2, Springer-Verlag, New York, 1970.

Roelof, E. C., and D. J. Williams, The terrestrial ring current: from in situ measurements to global images using energetic neutral atoms, *John Hopkins APL Tech. Dig., 9*, 144-163, 1988.

Schulz, M., L., and J. Lanzerotti, Physics and chemistry in space, vol. 7, *Particle Diffusion in the Radiation Belts*, chap. 2, Springer, New York, 1974.

Shelley, E. G., D. M. Klumpar, W. K. Peterson, A. Ghielmetti, H. Balsiger, K. Geiss, and H. Rosenbauer, AMPTE/CCE observations of the plasma composition below 17 keV during the September 4, 1984 magnetic storm, *Geophys. Res. Lett., 12*, 321-324, 1985.

Slater, D. W., and E. W. Kleckner, Occurrences of stable auroral red arcs detected by the Pacific Northwest Laboratory Photometer Network, 1978-1988, *Rep. PNL-7184*, Pac. Northwest Lab., Richland, Wash., 1989.

Spitzer, L., *Physics of Fully Ionized Gases*, 2nd ed., chap. 5, Interscience, New York, 1962.

Spjeldvik, W. N., Equilibrium structure of equatorially mirroring radiation belt protons, *J. Geophys. Res., 82*, 2801-2808, 1977.

Stern, D. P., The motion of a proton in the equatorial magnetosphere, *J. Geophys. Res., 80*, 595-599, 1975.

Tulunay, Y. K., and J. Sayers, Characteristics of the mid-latitude trough as determined by the electron density experiment on ARIEL-3, *J. Atmos. Terr. Phys., 33*, 1737-1761, 1971.

Volland, H., A semiempirical model of large-scale magnetospheric electric fields, *J. Geophys. Res., 78*, 171-180, 1973.

Wentworth, R. C., W. M. MacDonald, and S. F. Singer, Lifetimes of trapped radiation belt particles determined by Coulomb scattering, *Phys. Fluids, 2*, 499-509, 1959.

Williams, D. J., T. A. Fritz, and A. Konradi, Observations of proton spectra ($1.0 \leq E_p \leq 300$ keV) and fluxes at the plasmapause, *J. Geophys. Res., 78*, 4751-4755, 1973.

Young, E. R., D. G. Torr, P. Richards, and A. F. Nagy, A computer simulation of the mid-latitude plasmasphere and ionosphere, *Planet. Space Sci., 28*, 881-893, 1980.

M.-C. Fok, G. V. Khazanov, J. U. Kozyra, A. F. Nagy, and C. E. Rasmussen, Space Physics Research Laboratory, Department of Atmospheric, Oceanic and Space Sciences, University of Michigan, Ann Arbor, MI 48109.

(Received January 7, 1993;
revised May 3, 1993;
accepted June 22, 1993.)